Supplementary Information

for paper

Investigation of slow magnetic relaxation in a series of 1D polymeric cyclobutane-1,1-dicarboxylates based on $Ln^{III}V^{IV}_2$ units (Ln^{III} = Tb, Dy, Ho, Er, Tm, Yb): rare examples of V^{IV}-4*f* single-molecule magnets

Evgeniya S. Bazhina,[a,*] Maxim A. Shmelev,[a] Natalia V. Gogoleva,[a] Konstantin A. Babeshkin,[a] Ivan V. Kurganskii,[b] Nikolay N. Efimov,[a] Matvey V. Fedin,[b] Mikhail A. Kiskin[a] and Igor L. Eremenko[a]

[a] N.S. Kurnakov Institute of General and Inorganic Chemistry of the Russian Academy of Sciences, Leninsky prosp. 31, Moscow 119991, Russian Federation

E-mail: bazhina@igic.ras.ru

[b] International Tomography Center, Siberian Branch of Russian Academy of Sciences, Institutskaya St. 3a, Novosibirsk 630090, Russian Federation

Table of contents

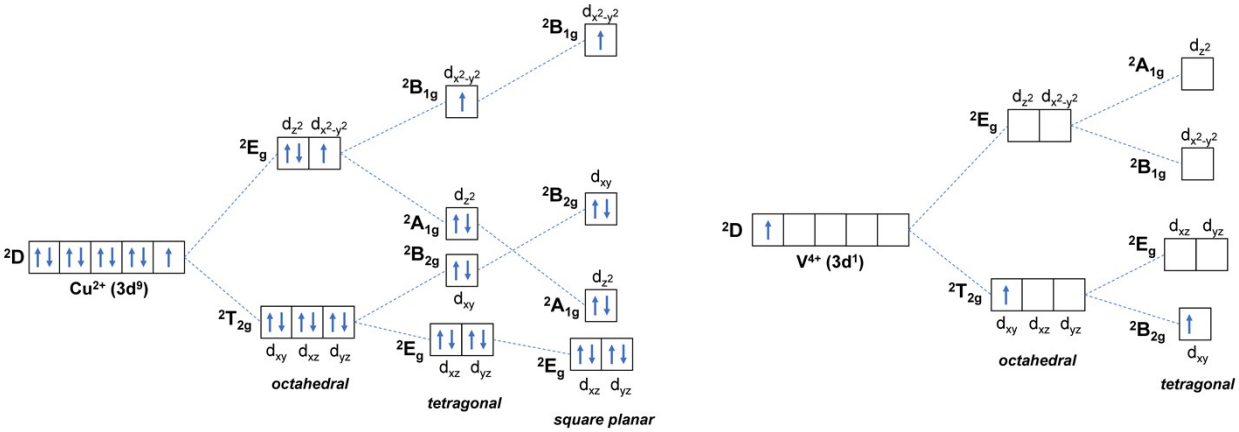

Figure S1. Splitting of the energy levels of Cu^{II} ($3d^9$) (left) and V^{IV} ($3d^1$) ion (right) in different crystal fields.

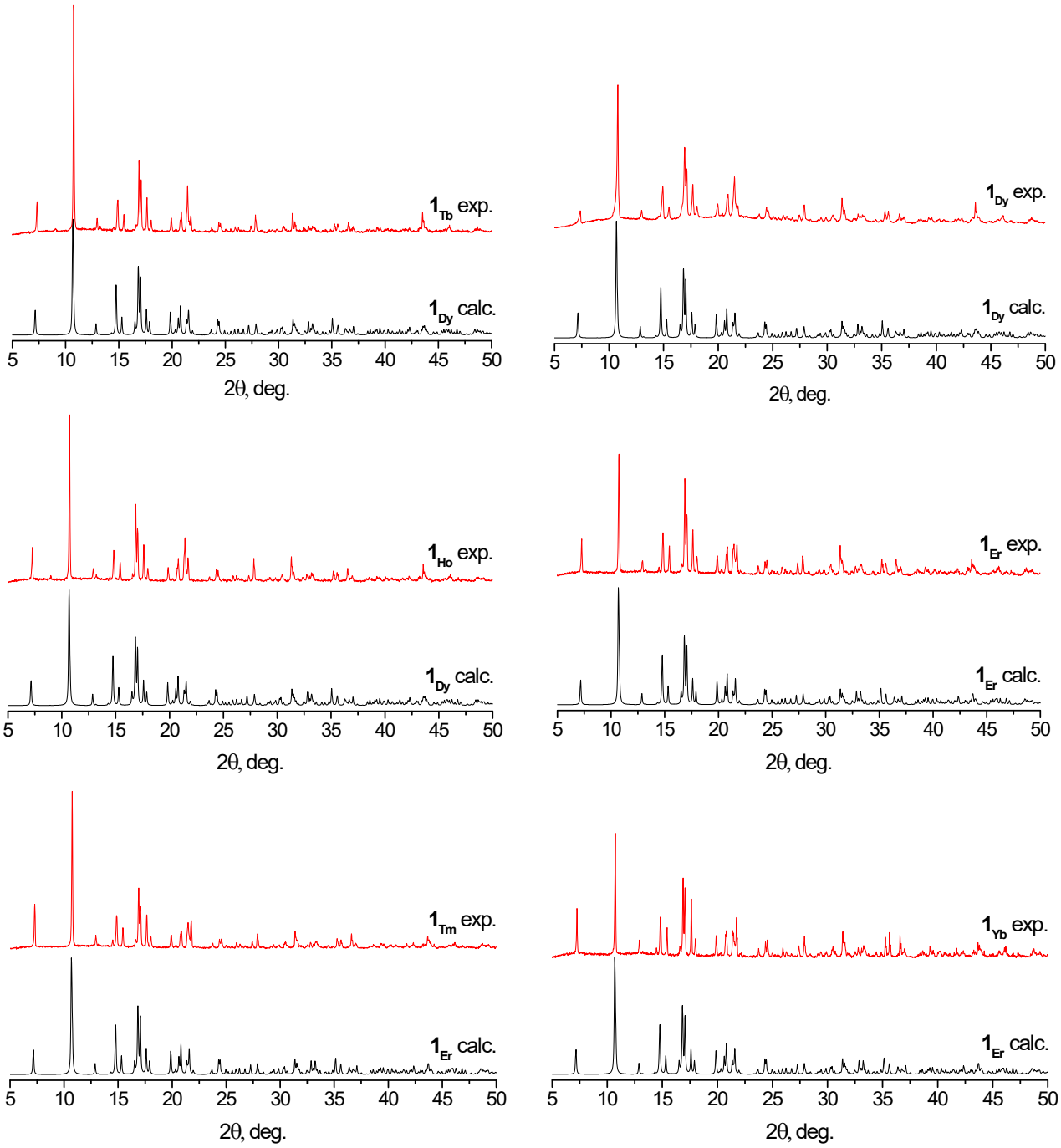

Figure S2. Experimental PXRD patterns for $\mathbf{1_{Ln}}$ measured at 295 K and their comparison with calculated data.

The description of crystal structures

Table S1. Continuous shape measures (CShM) for DyO_8 and ErO_8 coordination polyhedra in compounds $\mathbf{1_{Dy}}$ and $\mathbf{1_{Er}}$. The lowest SHAPE values are shown highlighted indicating best fits.

Structure ML_8	**SAPR-8**	**TDD-8**	**JBTPR-8**	**BTPR-8**	**JSD-8**
$\mathbf{1_{Dy}}$	1.556	**0.630**	3.118	2.501	3.874
$\mathbf{1_{Er}}$	1.542	**0.640**	3.135	2.498	3.919

Codes: SAPR-8 (D4d) Square antiprism; TDD-8 (D2d) Triangular dodecahedron; JBTPR-8 (C2v) Biaugmented trigonal prism J50; BTPR-8 (C2v) Biaugmented trigonal prism; JSD-8 (D2d) Snub diphenoid J84.

Table S2. Selected bond angles (ω, deg.) for $\mathbf{1_{Dy}}$.

Angle	ω	Angle	ω
O10–Dy1–O10^{i}	143.81(10)	O12–Dy1–O13	120.00(9)
O10^{i}–Dy1–O13	68.11(8)	O12–Dy1–O13^{i}	132.00(8)
O10^{i}–Dy1–O13^{i}	147.31(7)	O12^{i}–Dy1–O13^{i}	120.00(9)
O10–Dy1–O13	147.31(7)	O12^{i}–Dy1–O13	132.00(8)
O10–Dy1–O13^{i}	68.11(8)	O12–Dy1–O12^{i}	78.45(12)
O10–Dy1–O11^{i}	90.65(8)	O12–Dy1–O11^{i}	71.58(8)
O10^{i}–Dy1–O11	90.65(8)	O12^{i}–Dy1–O11^{i}	149.65(8)
O10–Dy1–O11	102.00(8)	O12^{i}–Dy1–O11	71.58(8)
O10^{i}–Dy1–O11^{i}	102.00(8)	O12–Dy1–O11	149.65(8)
O13–Dy1–O13^{i}	82.02(12)	O11–Dy1–O13	78.87(9)
O12^{i}–Dy1–O10^{i}	75.18(8)	O11–Dy1–O13^{i}	70.14(8)
O12^{i}–Dy1–O10	76.97(8)	O11^{i}–Dy1–O13	70.14(8)
O12–Dy1–O10	75.18(8)	O11^{i}–Dy1–O13^{i}	78.87(9)
O12–Dy1–O10^{i}	76.97(8)	O11^{i}–Dy1–O11	138.66(12)

Symmetry code: (i) -x+1, y, -z+1/2.

Table S3. Selected bond angles (ω, deg.) for $\mathbf{1_{Er}}$.

Angle	ω	Angle	ω
O4W–Er1–O4W^{i}	78.8(2)	O8^{i}–Er1–O2W^{i}	90.29(14)
O4W^{i}–Er1–O8	75.30(13)	O8–Er1–O2W^{i}	102.12(14)
O4W–Er1–O8	77.24(13)	O8–Er1–O2W	90.29(14)
O4W^{i}–Er1–O8^{i}	77.24(13)	O8^{i}–Er1–O2W	102.12(14)
O4W–Er1–O8^{i}	75.30(13)	O8–Er1–O3W	146.96(13)
O4W^{i}–Er1–O2W^{i}	149.63(14)	O8^{i}–Er1–O3W	68.04(13)
O4W^{i}–Er1–O2W	71.21(14)	O8–Er1–O3W^{i}	68.04(13)
O4W–Er1–O2W^{i}	71.20(14)	O8^{i}–Er1–O3W^{i}	146.96(13)
O4W–Er1–O2W	149.64(14)	O2W–Er1–O2W^{i}	139.0(2)
O4W^{i}–Er1–O3W	119.92(15)	O2W–Er1–O3W	70.31(15)
O4W^{i}–Er1–O3W^{i}	132.01(14)	O2W–Er1–O3W^{i}	78.93(15)
O4W–Er1–O3W	132.01(14)	O2W^{i}–Er1–O3W^{i}	70.31(15)
O4W–Er1–O3W^{i}	119.92(15)	O2W^{i}–Er1–O3W	78.93(15)
O8^{i}–Er1–O8	144.23(17)	O3W–Er1–O3W^{i}	81.8(2)

Symmetry code: (i) -*x*+1, *y*, -*z*+1/2.

Table S4. Hydrogen bonding parameters of structure $\mathbf{1_{Dy}}$.

Fragment D–H···A	Distance/ Å			D–H···A /°
	D–H	H···A	D···A	
O2–H2A···O6^{i}	0.84	1.98	2.774(4)	158
O2–H2B···O8^{ii}	0.74	2.03	2.741(3)	162
O3–H3A···O6^{iii}	0.86	1.96	2.712(4)	147
O3–H3B···O4	0.88	2.02	2.815(4)	149
O11–H11A···O4^{iv}	0.80	2.00	2.798(3)	176
O11–H11B···O1^{v}	0.79	1.97	2.764(3)	174
O12–H12A···O8^{vi}	0.84	1.87	2.703(3)	172
O12–H12B···O9	0.80	2.03	2.718(3)	144
O13–H13A···O10^{i}	0.83	2.35	2.658(3)	103
O13–H13B···O3^{iv}	0.85	1.79	2.633(3)	174
C4–H4A···O6	0.99	2.47	2.850(4)	102
C6–H6A···O4^{vii}	0.99	2.60	3.453(4)	145
C12–H12C···O8	0.99	2.49	2.855(4)	101
C12–H12D···O10	0.99	2.43	2.808(5)	102

Symmetry codes: (i) 1-x, y, 1/2-z; (ii) x, y, 1/2-z; (iii) 1+x, y, z; (iv) 1/2-x, -1/2+y, 1/2-z; (v) x, 1-y, -1/2+z; (vi) 1+x, y, z; (vii) 1/2-x, 3/2-y, 1-z.

Table S5. Hydrogen bonding parameters of structure $\mathbf{1_{Er}}$.

Fragment D–H···A	Distance/ Å			D–H···A /°
	D–H	H···A	D···A	
O1W–H1WB···O2^{i}	0.98	1.80	2.761(6)	164
O5W–H1WA···O2^{i}	0.92	1.80	2.708(6)	170
O5W–H1WB···O4^{ii}	0.84	2.26	2.816(5)	124
O4W–H1WA···O7^{i}	0.85	2.02	2.712(5)	137
O4W–H1WB···O6^{ii}	0.85	1.88	2.711(5)	165
O2W–H1WA···O9^{iii}	0.86	1.95	2.769(5)	160
O2W–H1WB···O4^{iv}	0.85	1.98	2.803(6)	161
O3W–H1WA···O5W^{iv}	0.85	1.88	2.623(6)	145
O3W–H1WB···O2W	0.85	2.36	2.729(6)	106
C4–H4B···O4^{v}	0.99	2.59	3.448(7)	144
C6–H6B···O2	0.99	2.48	2.852(7)	102
C12–H12A···O6	0.99	2.49	2.855(8)	101
C12–H12B···O8	0.99	2.42	2.801(8)	102

Symmetry codes: (i) 1-x, y, 1/2-z; (ii) x, y, 1/2-z; (iii) 1-x, 1-y, 1-z; (iv) 1/2+x, 1/2+y, z; (v) 1/2-x, 1/2-y, 1-z.

Magnetic properties

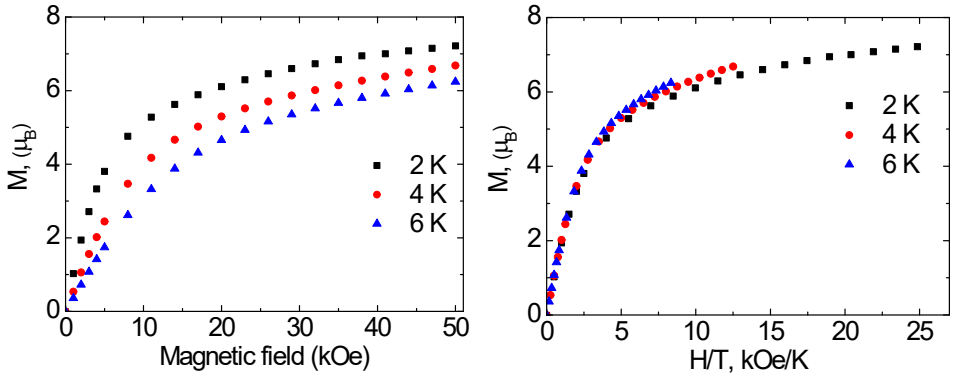

Figure S3. The magnetization M(*T*) (*left*) and M(H/*T*) (*right*) dependences at different temperatures for complex $\mathbf{1}_{\mathbf{Dy}}$.

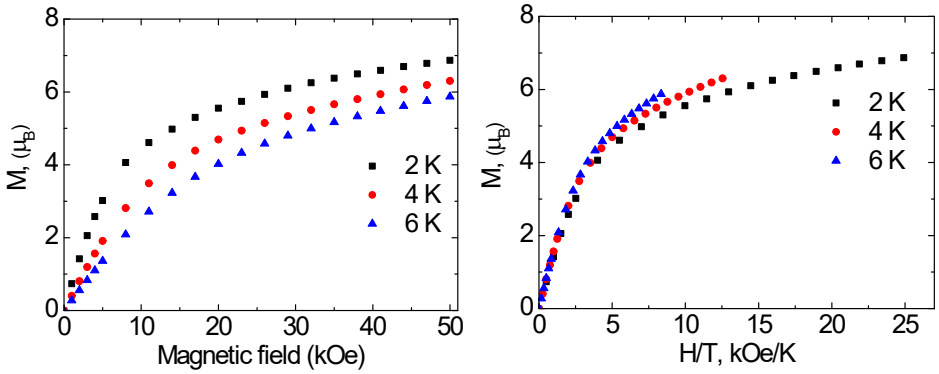

Figure S4. The magnetization M(*T*) (*left*) and M(H/*T*) (*right*) dependences at different temperatures for complex $\mathbf{1}_{\mathbf{Er}}$.

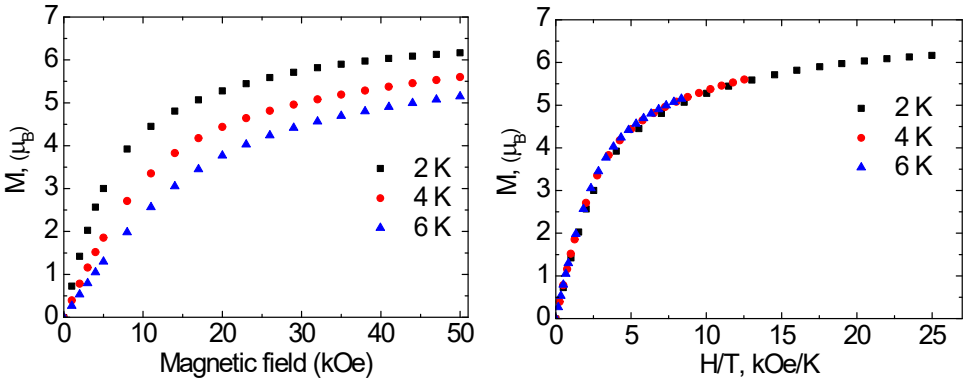

Figure S5. The magnetization M(*T*) (*left*) and M(H/*T*) (*right*) dependences at different temperatures for complex $\mathbf{1}_{\mathbf{Tm}}$.

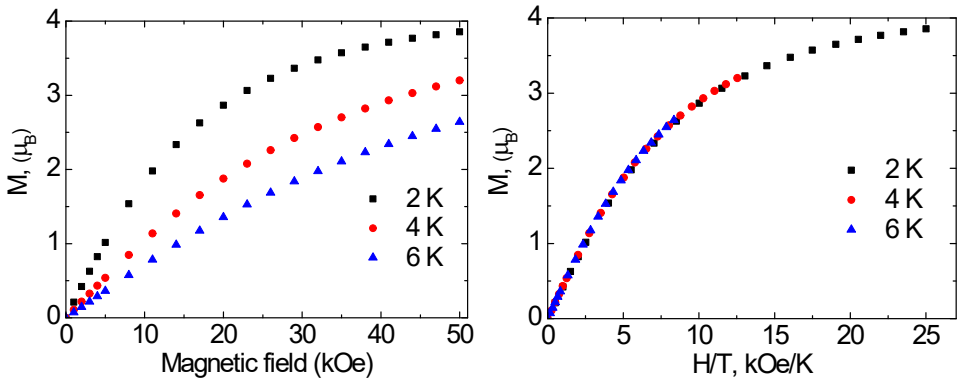

Figure S6. The magnetization M(*T*) (*left*) and M(H/*T*) (*right*) dependences at different temperatures for complex $\mathbf{1}_{\mathbf{Yb}}$.

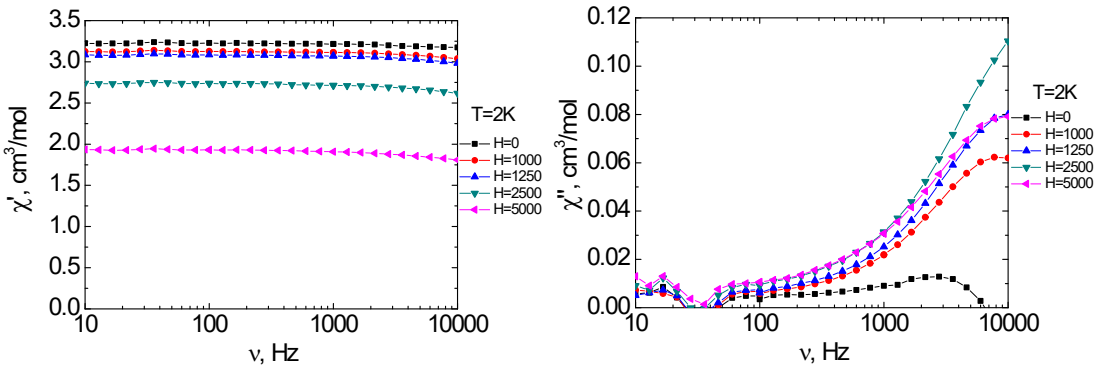

Figure S7. Frequency dependencies of the in-phase (χ') (*left*) and out-of-phase (χ'') (*right*) components of the dynamic magnetic susceptibility of $\mathbf{1_{Tb}}$ at varied strength of the external static magnetic field and T = 2 K. Solid lines are visual guides.

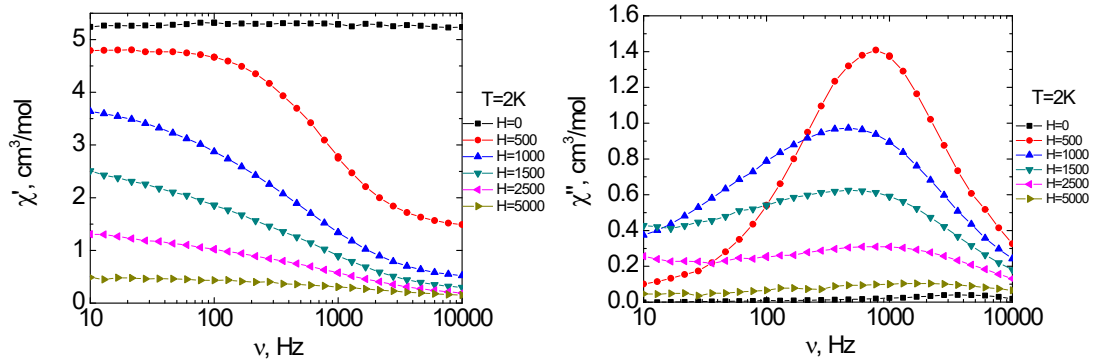

Figure S8. Frequency dependencies of the in-phase (χ') (*left*) and out-of-phase (χ'') (*right*) components of the dynamic magnetic susceptibility of $\mathbf{1_{Dy}}$ at varied strength of the external static magnetic field and T = 2 K. Solid lines are visual guides.

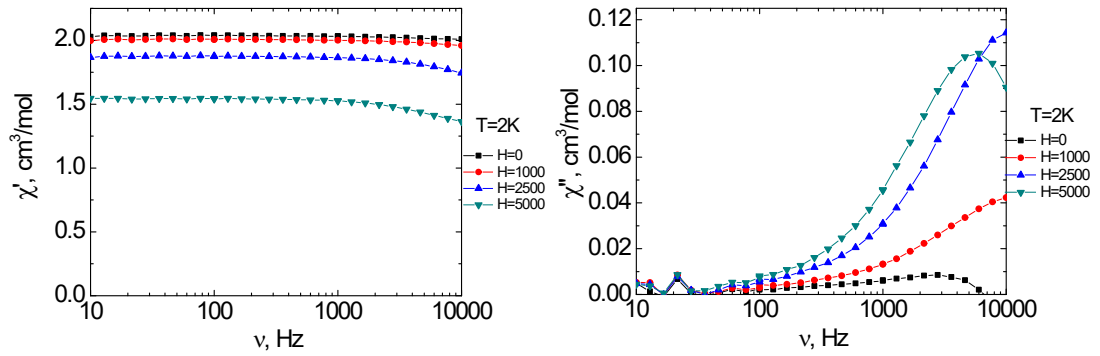

Figure S9. Frequency dependencies of the in-phase (χ') (*left*) and out-of-phase (χ'') (*right*) components of the dynamic magnetic susceptibility of $\mathbf{1_{Ho}}$ at varied strength of the external static magnetic field and T = 2 K. Solid lines are visual guides.

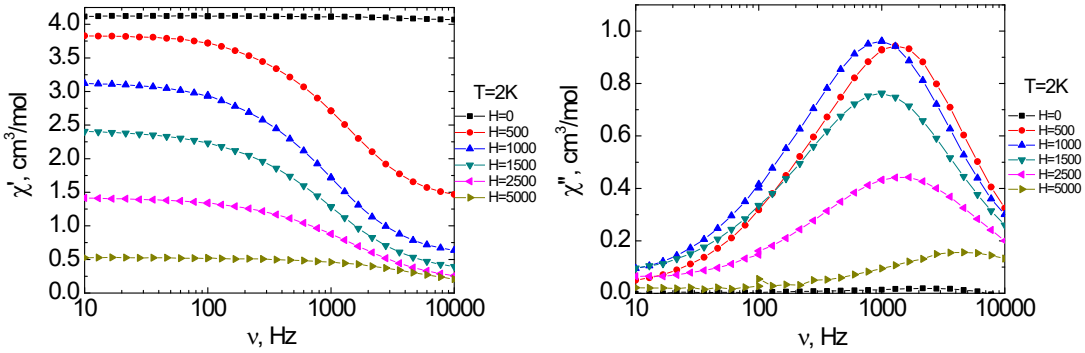

Figure S10. Frequency dependencies of the in-phase (χ') (*left*) and out-of-phase (χ'') (*right*) components of the dynamic magnetic susceptibility of $\mathbf{1_{Er}}$ at varied strength of the external static magnetic field and T = 2 K. Solid lines are visual guides.

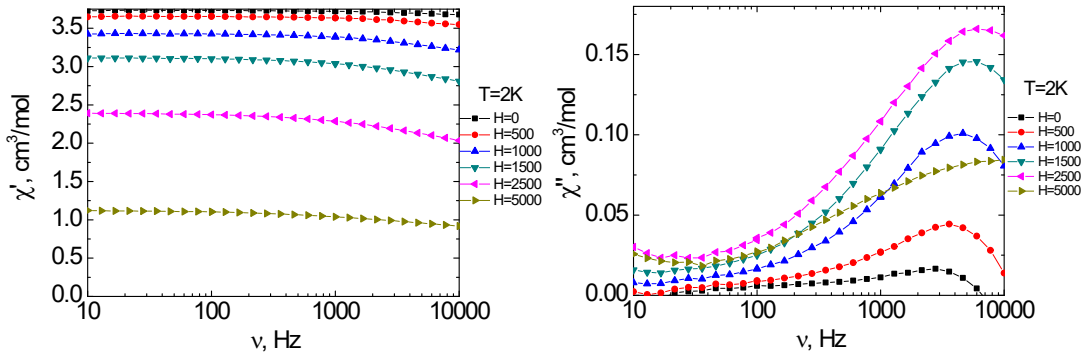

Figure S11. Frequency dependencies of the in-phase (χ') (*left*) and out-of-phase (χ'') (*right*) components of the dynamic magnetic susceptibility of $\mathbf{1_{Tm}}$ at varied strength of the external static magnetic field and T = 2 K. Solid lines are visual guides.

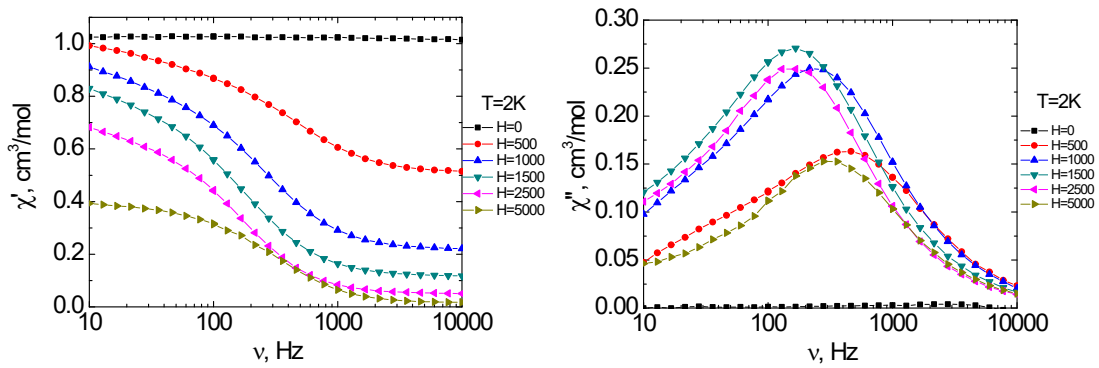

Figure S12. Frequency dependencies of the in-phase (χ') (*left*) and out-of-phase (χ'') (*right*) components of the dynamic magnetic susceptibility of $\mathbf{1_{Yb}}$ at varied strength of the external static magnetic field and T = 2 K. Solid lines are visual guides.

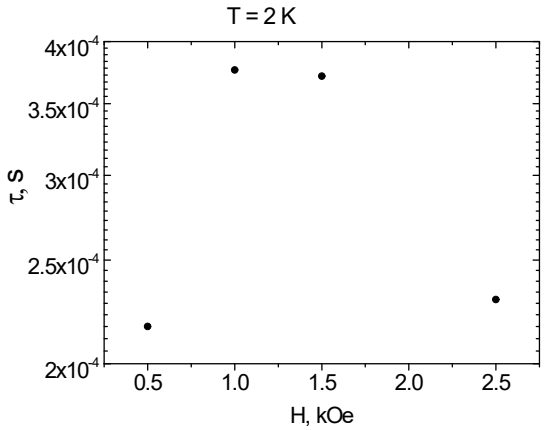

Figure S13. The τ vs. *H* plot for $\mathbf{1_{Dy}}$ at 2 K. The data corresponding to magnetic fields *H* = 0 and 5000 Oe is omitted because of low corresponding values.

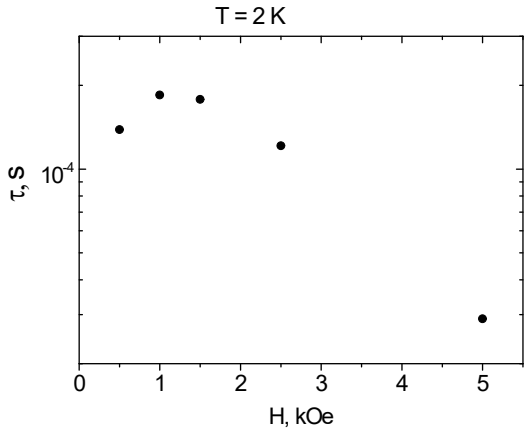

Figure S14. The τ vs. *H* plot for $\mathbf{1_{Er}}$ at 2 K. The data corresponding to magnetic field *H* = 0 is omitted because of low corresponding values.

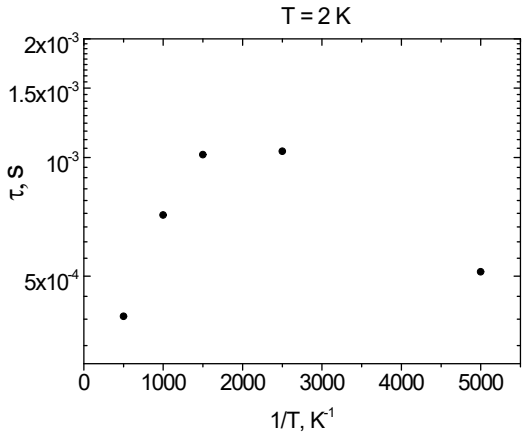

Figure S15. The τ vs. *H* plot for $\mathbf{1_{Yb}}$ at 2 K. The data corresponding to magnetic field *H* = 0 is omitted because of low corresponding values.

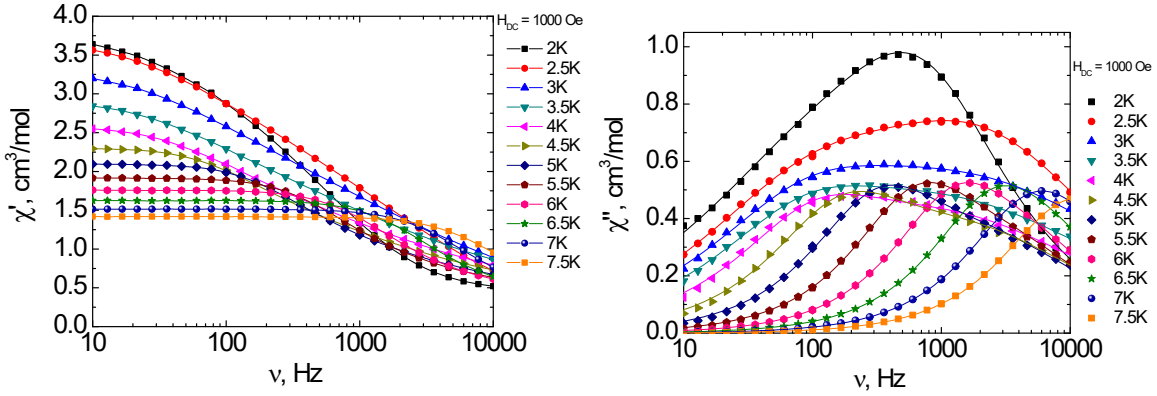

Figure S16. Frequency dependences of the in-phase χ′ (*left*) and out-of-phase χ″ (*right*) components of the *ac* susceptibility between 2 and 7.5 K for $\mathbf{1_{Dy}}$ under 1000 Oe *dc*-field. Solid lines are guides for the eyes (*left*), fits by the generalized Debye model for two relaxation processes (*right*).

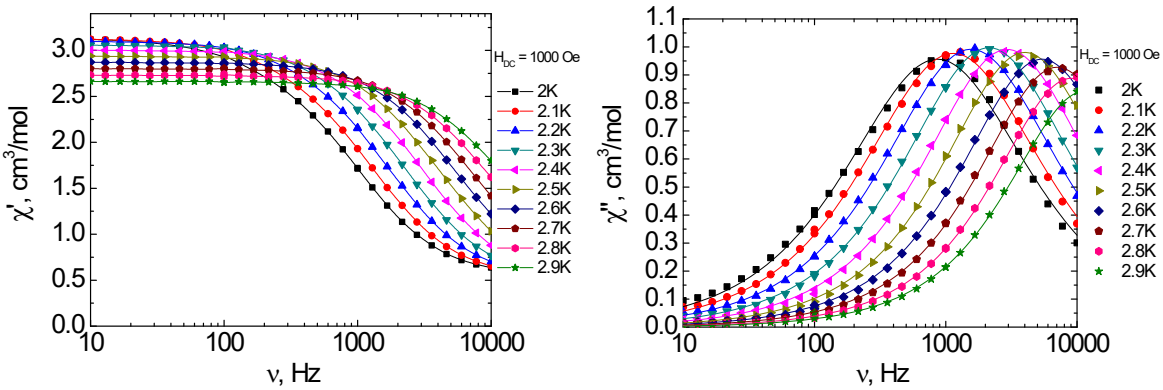

Figure S17. Frequency dependences of the in-phase χ′ (*left*) and out-of-phase χ″ (*right*) components of the *ac* susceptibility between 2 and 2.9 K for $\mathbf{1_{Er}}$ under 1000 Oe *dc*-field. Solid lines are guides for the eyes (*left*), fits by the generalized Debye model (*right*).

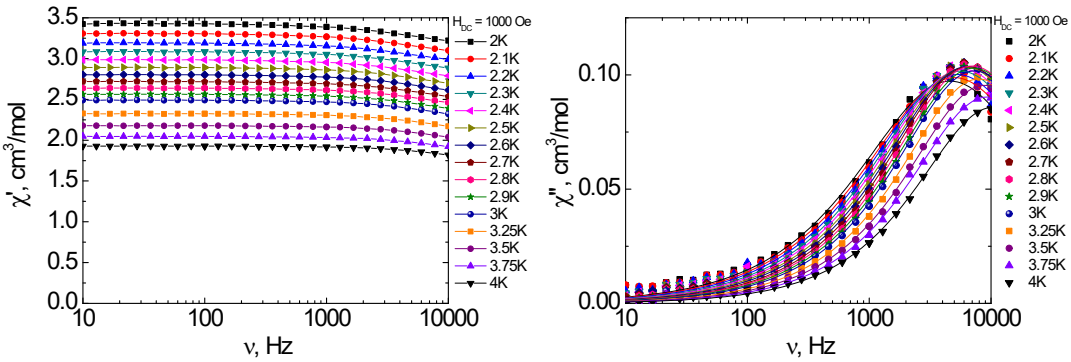

Figure S18. Frequency dependences of the in-phase χ′ (*left*) and out-of-phase χ″ (*right*) components of the *ac* susceptibility between 2 and 4 K for $\mathbf{1_{Tm}}$ under 1000 Oe *dc*-field. Solid lines are guides for the eyes (*left*), fits by the generalized Debye model (*right*).

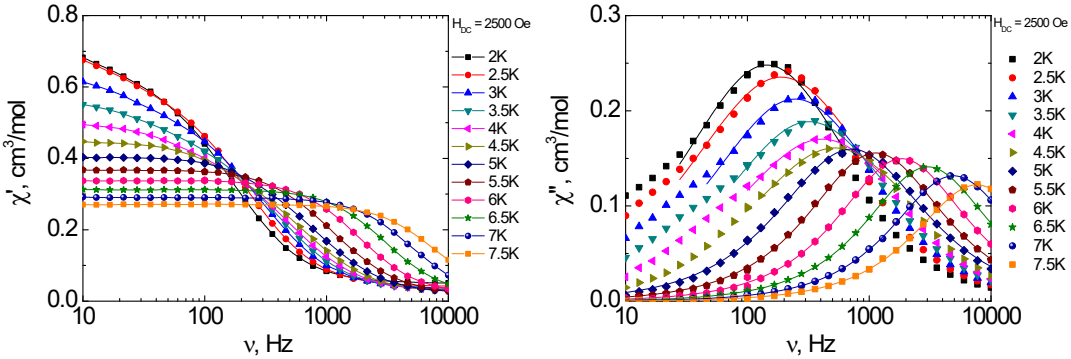

Figure S19. Frequency dependences of the in-phase χ′ (*left*) and out-of-phase χ″ (*right*) components of the *ac* susceptibility between 2 and 7.5 K for $\mathbf{1_{Yb}}$ in 2500 Oe *dc*-field. Solid lines are guides for the eyes (*left*), fits by the generalized Debye model (*right*).

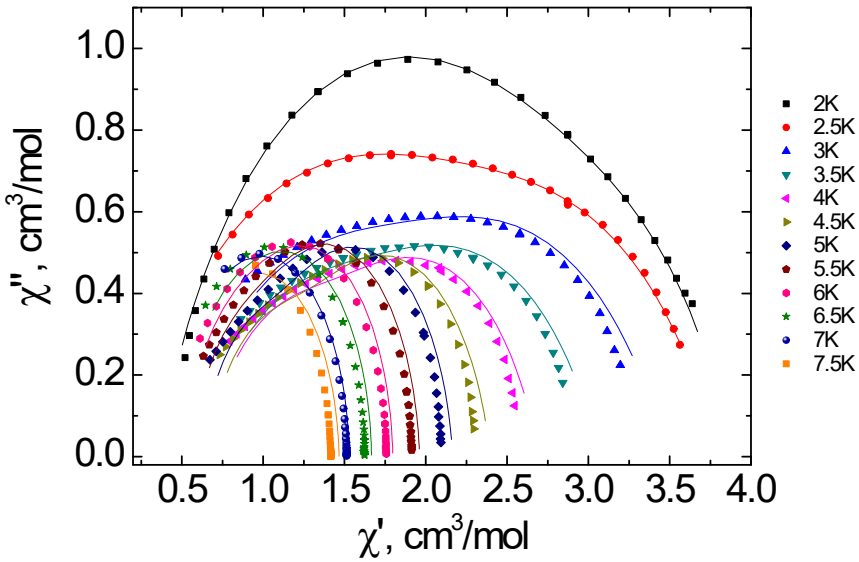

Figure S20. Cole-Cole plots for $\mathbf{1_{Dy}}$ measured at 2-7.5 K. The lines represent the fit using the MagSuite v.3.2 software [M. Rouzières, Zenodo (2023); https://doi.org/10.5281/zenodo.4030310].

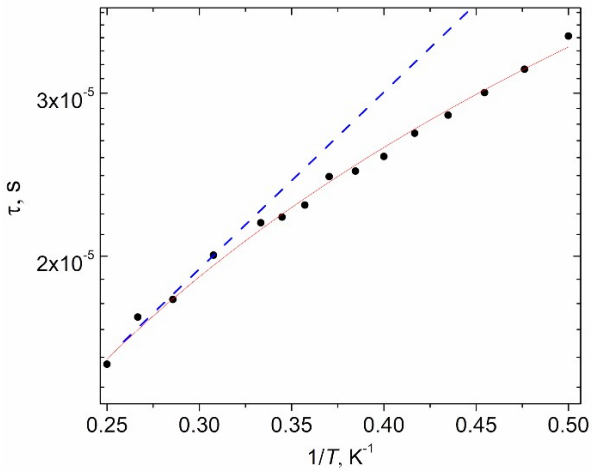

Figure S21. The τ vs. 1/*T* plots for $\mathbf{1_{Tm}}$ under 1000 Oe field. Blue dotted line represents the fitting of a high-temperature range by the Orbach mechanism. Red solid line represents the fitting by the Raman relaxation mechanism.

Table S6. The best-fit parameters of magnetization relaxation for $\mathbf{1_{Tm}}$.

Compound	Orbach		Raman + direct			Raman	
	Δ_{eff}/k_B, K	τ_0, s	A_{direct}, $K^{-1}Oe^{-4}s^{-1}$	C_{Raman}, $s^{-1}K^{-n\_Raman}$	n_{Raman}	C_{Raman}, $c^{-1}K^{-n\_Raman}$	n_{Raman}
$\mathbf{1_{Tm}}$	4.4	$5.2\cdot10^{-6}$	–	–	–	13672	1.12

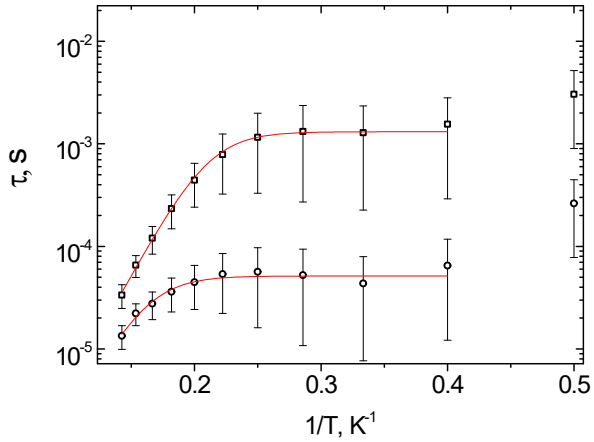

Figure S22. The τ vs. $1/T$ plots for $\mathbf{1_{Dy}}$ under 1000 Oe field with confidence intervals. Red solid lines represent the fittings in the whole temperature range by the sum of the Orbach and QTM relaxation mechanisms.

Table S7. The best-fit parameters of magnetization relaxation for $\mathbf{1_{Dy}}$ (MagSuite Cole-Cole fit).

	Orbach + QTM		
	Δ_{eff}/k_B, K	τ_0, s	B, s^{-1}
LF	52 ± 2	$2.1\cdot10^{-8} \pm 5\cdot10^{-9}$	762 ± 52
HF	52 (fixed)	$1.14\cdot10^{-8} \pm 7\cdot10^{-10}$	19447 ± 1020

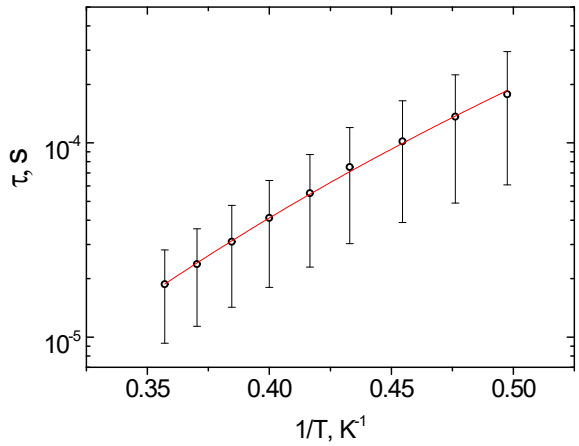

Figure S23 The τ vs. $1/T$ plots for $\mathbf{1_{Er}}$ under 1000 Oe field with confidence intervals. Red solid line represents the fittings in the whole temperature range by the Raman relaxation mechanism.

Table S8. The best-fit parameters of magnetization relaxation for $\mathbf{1_{Er}}$ (MagSuite Cole-Cole fit).

Compound	Raman	
	C_{Raman}, $c^{-1}K^{-n\_Raman}$	n_{Raman}
$\mathbf{1_{Er}}$	43.0 ± 3	6.92 ±0.09

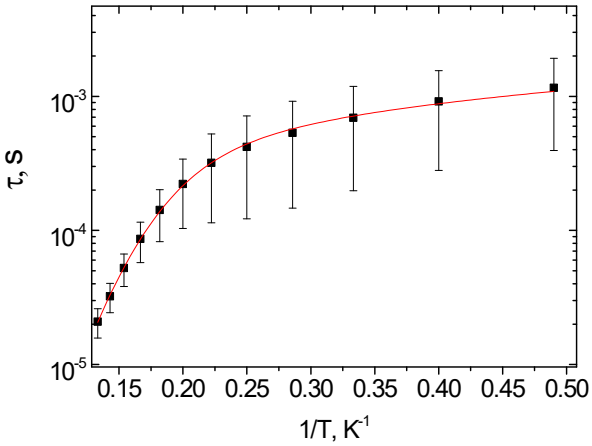

Figure S24. The τ vs. 1/*T* plots for $\mathbf{1_{Yb}}$ under 2500 Oe field with confidence intervals. Red solid lines represent the fittings in the whole temperature range by the sum of the Raman and direct relaxation mechanisms.

Table S9. The best-fit parameters of magnetization relaxation for $\mathbf{1_{Yb}}$ (MagSuite Cole-Cole fit).

Compound	**Raman + direct**		
	A_{direct}, $K^{-1}Oe^{-4}s^{-1}$	C_{Raman}, $s^{-1}K^{-n\_Raman}$	n_{Raman}
$\mathbf{1_{Yb}}$	$1.15\cdot10^{-11} \pm 3\cdot10^{-13}$	$2.1\cdot10^{-2} \pm 5\cdot10^{-3}$	7.2 ± 0.1

EPR Spectroscopy

Figure S25 shows CW EPR spectra for two complexes of V^{4+} with diamagnetic Y^{3+} ion. One complex $\mathbf{1_Y}$ has a 1D-polymeric structure similar to $\mathbf{1_{Yb}}$ and $\mathbf{1_{Dy}}$ complexes, another one has a molecular structure ($\mathbf{M_Y}$); both of them were studied in our previous work [16]. CW EPR spectra of $\mathbf{1_Y}$ and $\mathbf{M_Y}$ are very similar; they can be simulated using close sets of parameters g = [1.974 1.974 1.938] and A = [184 184 518] MHz ($\mathbf{1_Y}$), and g = [1.975 1.975 1.938] and A = [183 183 519] MHz ($\mathbf{M_Y}$), thus reflecting similar local environment of V^{4+} ions. Both $T_m(T)$ dependences for $\mathbf{M_Y}$ and for $\mathbf{1_Y}$ have no peculiarity and show monotonic behavior; however, absolute values of T_m for $\mathbf{1_Y}$ were found shorter. Thus, with additional verifications, $\mathbf{M_Y}$ was used as a reference in Figure 7.

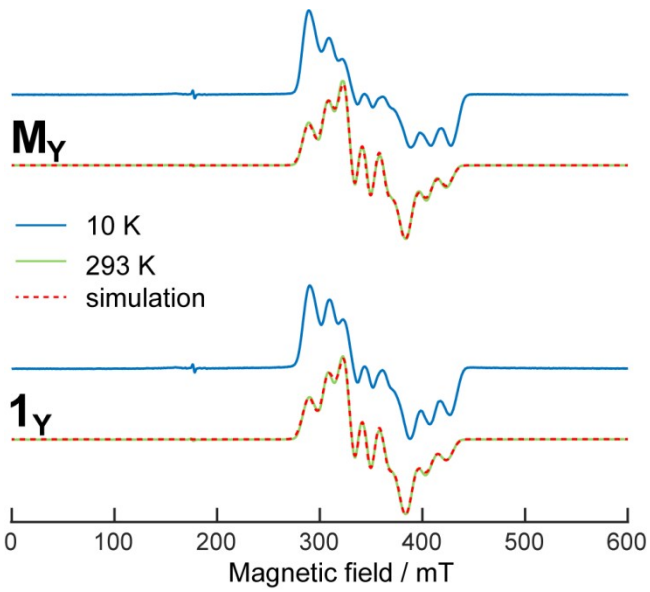

Figure S25. CW EPR spectra of $\mathbf{M_Y}$ and $\mathbf{1_Y}$ at 293 K and 10 K. Simulations are shown in red.

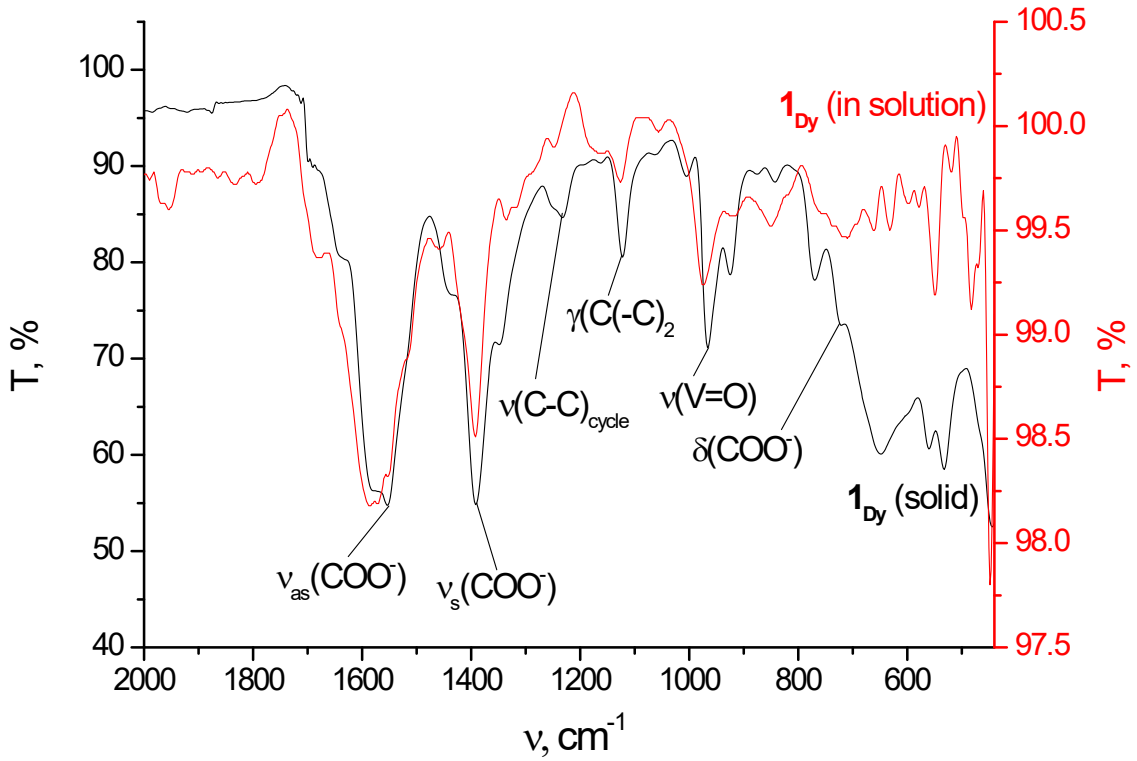

Figure S26. The IR spectra (fingerprint region) of solid sample (black line) and aqueous solution (red line) of compound $\mathbf{1_{Dy}}$.